Scientific Research Publishing

International Journal of Geosciences, 2026, 17(11), 951-975
https://www.scirp.org/journal/ijg
ISSN Online: 2156-8367
ISSN Print: 2156-8359

Hydrothermal Alteration and Gold Mineralization at the Toéyoko Prospect, a Satellite of the Bomboré Deposit (Burkina Faso)

Madi Ouedraogo[1*], Gounwendmanaghré Hubert Zongo[1], Pascal Ouiya[2], Ernest Gomdebziige Ouedraogo[1], Saga Sawadogo[3], Seta Naba[3]

[1]Department of Mining Engineering, Université Yembila Abdoulaye TOGUYENI, Fada N'Gourma, Burkina Faso
[2]Higher Teacher Training School (École Normale Supérieure), Institute of Training and Research in Science and Technology, Ouagadougou, Burkina Faso
[3]Geosciences and Environment Laboratory, Joseph Ki-Zerbo University, Ouagadougou, Burkina Faso
Email: *madisance1983@gmail.com

How to cite this paper: Ouedraogo, M., Zongo, G.H., Ouiya, P., Ouedraogo, E.G., Sawadogo, S. and Naba, S. (2026) Hydrothermal Alteration and Gold Mineralization at the Toéyoko Prospect, a Satellite of the Bomboré Deposit (Burkina Faso). *International Journal of Geosciences*, **17**, 951-975.
https://doi.org/10.4236/ijg.2026.1711044

Received: October 29, 2026
Accepted: November 23, 2026
Published: November 26, 2026

Copyright © 2026 by author(s) and Scientific Research Publishing Inc.
This work is licensed under the Creative Commons Attribution International License (CC BY 4.0).
http://creativecommons.org/licenses/by/4.0/

Open Access

Abstract

At the Toéyoko prospect (Bomboré district, Burkina Faso), gold is hosted by silicified and deformed granitoids cut by NNW-SSE shear zones; granitoid accounts for 93% of the core length grading at least 0.5 g/t Au. Alteration was characterized on 13 drill-core samples collected in pairs (mineralized and least altered) from six holes, using alteration indices, isocon mass balances and rank correlations; the Zr/TiO_2 ratio links each altered rock to a reference rock of the same family. The mineralized granitoids gained Na_2O (+18% to +40%), CO_2, S, As, Sb, Te and Ag, and lost K_2O (−67% to −94%), Rb and Ba; their molar Na/Al ratios (0.77 - 0.91) approach albite, and iron remained nearly constant. A second reference rock and an isocon defined by Ti and Al alone confirm the direction of these transfers; only the magnitude of the K loss depends on the reference rock. A mineralized metagabbro gained mainly silica and carbonate. Gold (0.84 - 8.64 g/t, versus ≤ 0.015 g/t elsewhere) increases with As, S and Na/Al and decreases with K_2O. This sodic, carbonate and sulfide alteration is consistent with a reduced aqueous-carbonic fluid, and gold probably precipitated through sulfidation of host-rock iron. Thresholds of As > 1000 ppm and S > 0.4%, refined by Na/Al ≥ 0.75 in the granitoids, separate the gold-bearing from the barren samples of this dataset.

Keywords

Orogenic Gold, Albitization, Sulfidation, Mass Balance, Birimian

1. Introduction

Orogenic gold deposits are surrounded by hydrothermal alteration haloes that often extend beyond the orebodies. These haloes form when the wall rocks react with reduced, low-salinity, sulfur-bearing aqueous-carbonic fluids in which gold is transported mainly as bisulfide complexes [1]-[3]. Whether these fluids are metamorphic or magmatic in origin is still debated [4] [5]. The haloes record additions of CO_2, S, K or Na, and of elements, such as As, Sb, Te, W and Bi; their geometry provides exploration vectors [6]. Gold commonly precipitates when the Fe-bearing minerals of the host rock are sulfidized [7].

The Baoulé-Mossi domain of the West African Craton is one of the main Paleoproterozoic gold provinces [8]-[10]. The Bomboré deposit hosts disseminated mineralization associated with albite, calcite, tourmaline, biotite and pyrite alteration [11] [12]. South of the deposit, at the Toéyoko prospect (P17 and P17 South showings), gold occurs mainly in silicified and deformed granitoids, but the associated alteration has not yet been quantified.

This paper has three aims: 1) to quantify the mass transfers associated with gold by comparing each altered rock with a reference rock, that is, a least-altered sample of the same rock type that stands for the rock before alteration; 2) to identify the pathfinder elements of the mineralization and their relationship with gold grades; and 3) to derive from these a zoning model and simple geochemical criteria for exploration.

2. Geological Setting

2.1. Regional Framework

The Baoulé-Mossi domain, which covers most of Burkina Faso, consists of volcano-sedimentary greenstone belts and granitoid batholiths emplaced between about 2.2 and 2.07 Ga [13]. These Birimian terranes were deformed during the Eburnean orogeny, whose transcurrent stage is associated with most gold deposits [14] [15]. They are cut by an anastomosing network of transpressional shear zones that channelled the ore fluids [16] [17]; in Burkina Faso, the large deposits lie along corridors such as the Tiébélé-Dori-Markoye corridor.

2.2. The Toéyoko Prospect

The Bomboré deposit, about 85 km east of Ouagadougou, is hosted by a greenstone belt 1 to 3 km wide and about 14 km long that belongs to the Tiébélé-Dori-Markoye corridor [11] [12]. The Toéyoko prospect is its southern extension (**Figure 1**). The host rocks are tholeiitic metagabbros, metasediments (arenites, metagreywackes, graphitic metapelites) and granitoids, all metamorphosed under greenschist-facies conditions; biotite granite plutons border the area to the west and south. The sampled sector lies at the southern end of the Bomboré corridor.

The main foliation, trending N-S to NNE, is subvertical at surface (015/82) and dips about 60˚ east at depth (mean plane 091/58); it is cut at a low angle by NNW-SSE shear zones (075/61) that carry most of the quartz veins [18]. The field name

"granodiorite" is kept on the maps; in the text these rocks are called "granitoids" because their composition is mostly tonalitic to trondhjemitic. This major-element classification remains provisional, as alteration may have modified it [18].

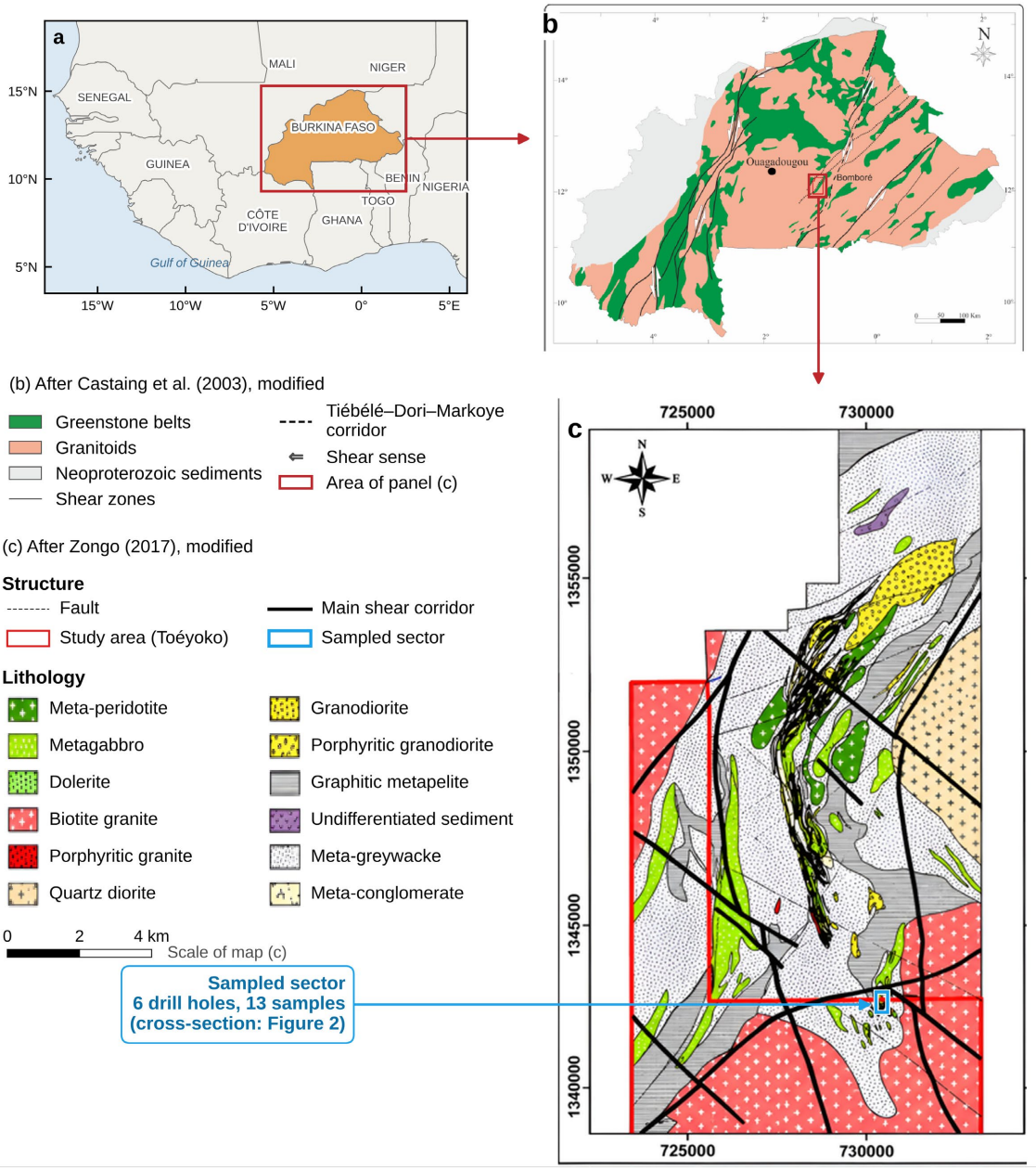

Figure 1. Location of the study area. (a) West Africa and Burkina Faso; (b) geological map of Burkina Faso showing the Bomboré district (red outline), modified from [19]; (c) geological map of the Bomboré district, modified from [11], showing the Toéyoko study area (red outline) and the sector of the six sampled drill holes (blue rectangle), shown in cross-section in **Figure 2**. UTM coordinates, zone 30N, WGS 84.

3. Materials and Methods

3.1. Samples and Drill-Hole Data

Thirteen diamond drill-core samples (intervals of about 1 m, between 45 and 169

m downhole, *i.e.*, about 35 to 129 m vertical depth, in fresh rock) were collected from six drill holes: four metagabbros (GB1 - GB4), eight granitoids (GR1 - GR8) and one arenite (AR1) (Table 1; Figure 2). In each of the six holes, an altered or mineralized rock was paired with a less altered rock of the same type located less than 20 m away downhole; arenite AR1 is a single sample. The rock type of each sample was checked on core before sampling and then refined by geochemical analysis [18]. The sampling was deliberate: it covers the three lithologies and both mineralized and barren intervals, but it is not a statistically representative set for the prospect.

Table 1. Analysed samples: location, rock type, alteration class and gold grade of the interval.

Sample	Drill hole	Interval (m)	Vert. depth (m)	Rock	Class	Au (g/t)
GB1	TYD0036	97 - 98	72	Metagabbro	LA	0.001
GB2	TYD0036	89 - 90	66	Differentiated/silicified metagabbro, carbonate-altered	SA	0.837
GB3	TYD0110	107 - 108	100	Metagabbro	LA	0.001
GB4	TYD0110	89 - 90	83	Differentiated/silicified metagabbro	MA	8.12
GR1	BBD1000	152 - 153	116	Granitoid, suite B	SA	8.64
GR2	TYD0046	63.6 - 64.7	48	Granitoid, suite A	SA	1.14
GR3	BBD1048	79 - 80	≈ 61	Granitoid, suite B	SA	5.82
GR4	BBD1000	168 - 169	129	Granitoid, suite B	LA	0.001
GR5	TYD0046	67 - 68	51	Granitoid, suite A	LA	0.001
GR6	TYD0023	45 - 46	35	Granitoid, suite B	LA	0.015
GR7	BBD1048	61 - 62	≈ 47	Granitoid, suite B	C	0.001
GR8	TYD0023	46 - 47	35	Granitoid, suite B	SA	5.15
AR1	TYD0023	84 - 85	64	Arenite (greywacke)	LA	0.002

Intervals measured downhole. Vert. depth: vertical depth of the interval midpoint, calculated from downhole surveys (≈: BBD1048, design orientation 270/−50). Classes: SA, strongly altered (As > 2000 ppm and S > 0.7%); MA, moderately altered; C, carbonate-altered, As-poor; LA, least altered (As < 400 ppm and S < 0.25%). GR4 is weakly carbonate-altered (CSI = 0.26).

The eight granitoids do not form a homogeneous group. Their Zr/TiO_2 ratio, which is little affected by hydrothermal alteration, divides them into two groups with different original compositions, referred to here as "suites": suite A (GR2, GR5) is Zr-poor ($Zr/TiO_2 \approx 134$ - 143) and suite B (GR1, GR3, GR4, GR6, GR7, GR8) is Zr-rich ($Zr/TiO_2 \approx 295$ - 549). These are the two suites defined in [18], where suite A is characterized by high Sr/Y and suite B by low Al and high Zr and Y. The suites may correspond to two intrusions or to two facies of the granitoid; they do not reflect two degrees of alteration, and each altered rock is compared only with

a reference rock from the same suite. Suite A comes from a single drill hole (TYD0046), and four of the six suite B granitoids come from holes BBD1000 and BBD1048, north of the Toéyoko holes. GR2 and GR5 are logged as metasediments (S3) in the drill log, and portable X-ray fluorescence does not distinguish them from metasediments. Re-examination of the core before sampling identified them as fine-grained granitoids, and their CIPW norms and trace elements place them with the granitoids [18].

To place the samples within the gold distribution, fire-assay grades and lithological logs from eleven drill holes in the area were compiled: 1513 intervals, or 1527 m of core. Mineralized intercepts are defined by a cut-off grade of 0.5 g/t Au, a maximum internal dilution of 2 m and a minimum length of 2 m.

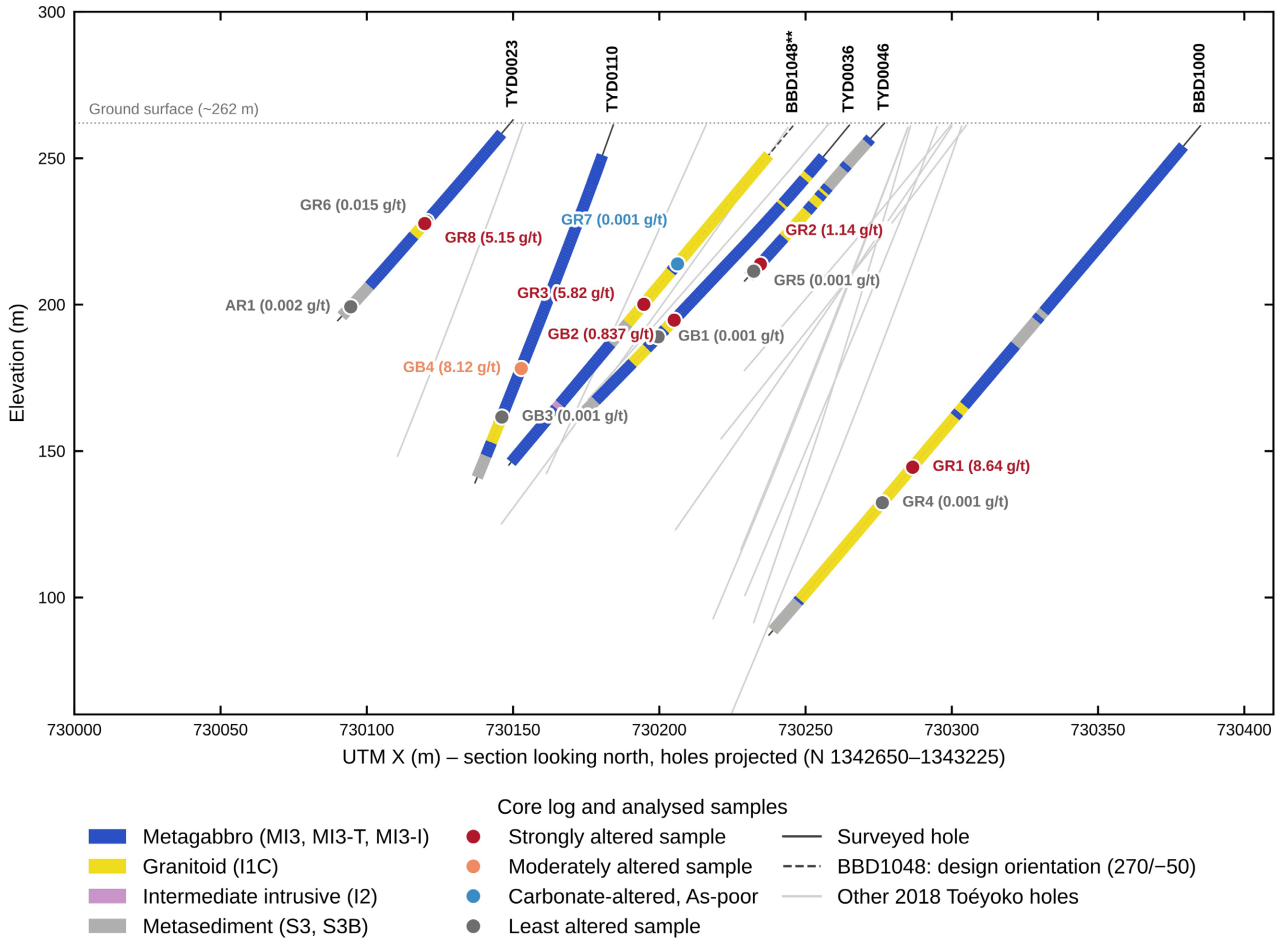

Figure 2. W-E cross-section of the sampled sector (looking north; holes projected between N 1,342,650 and N 1,343,225), showing the lithological logs and the sample locations, coloured by alteration class (**Table 1**) and labelled with their gold grade. **BBD1048: collar placed on the section by correlating the granitoid-metasediment contact with BBD1000, using the design orientation (270/−50). Light grey: other 2018 drill holes.

3.2. Chemical Analyses and Quality Control

Analyses were performed by SGS South Africa (Randfontein; laboratory accredited to ISO/IEC 17025 by SANAS, No. T0265; certificate RFT24-65463); methods

and detection limits are summarized in Table 2. Quality control relies on the laboratory's internal controls, analysed in the same batch: one blank, five certified reference materials and three duplicates (one per method). Accuracy was checked with the certified reference materials, taking agreement within two standard deviations of the certified value as the acceptance criterion. OREAS 907, certified for four-acid digestion, returned 90% to 112% of the certified values for the 25 certified elements checked, including Zr (252 against 239 ppm, 105%) and Hf (6.51 against 6.49 ppm, 100%); all lie within two standard deviations except K by ICP-OES (109%), which is not used here (K_2O is measured by XRF). CANMET SU-1b returned 98% to 104% of the certified values for Ag, Al, Mg and Mn. The blank is below or close to the detection limits (maximum value: 4 ppm Ba). The median difference between samples and their duplicates is 2%; it does not exceed 1.5% for the major elements, is 2% for C and 4.5% for S, and reaches 11% to 14% for As, Ag and Zr. Gold grades for the same 1 m intervals were obtained by fire assay (SGS).

Four-acid digestion does not fully dissolve zircon, so Zr and Hf contents are low. Assuming that this underestimation is similar in the altered rock and in its reference rock, Zr and Hf can still be used in the mass balances, which are based on ratios. Since the OREAS 907 values are certified for four-acid digestion, the good Zr and Hf recoveries show that the laboratory dissolved a consistent fraction of zircon, not that zircon was fully dissolved. Because the assumption of a similar recovery in the altered and reference rocks cannot be verified directly, the mass balances were also recalculated with an isocon defined by TiO_2 and Al_2O_3 only (Section 4.4).

Table 2. Analytical methods (SGS South Africa) and quality control.

Parameter	Method	Code	Detection limit
Major elements	X-ray fluorescence on fused bead	GO_XRF72	0.01%
Loss on ignition (LOI)	Ignition	G_PHY01V	—
Total C and S	Combustion, infrared detection	GE_CSA06V	0.005%
Trace elements (>40)	ICP-MS and ICP-OES after four-acid digestion	GE_IMS40Q12, GE_ICP40Q12	0.01 - 1 ppm[a]
Gold	Fire assay (1 m intervals)	—	0.001 g/t
Quality control	1 blank, 5 certified reference materials, 3 duplicates (one per method)	—	Median duplicate difference: 2%; OREAS 907: 90% - 112% of certified values (Zr 105%, Hf 100%)

[a]As: 1 ppm; Pb, Cu, Zr: 0.5 ppm; W: 0.1 ppm; Sb, Te, Mo: 0.05 ppm; Ag, Hf: 0.02 ppm; Bi: 0.01 ppm. As is not quantified above 10,000 ppm. Zr and Hf are underestimated (incomplete dissolution of zircon).

3.3. Data Processing

Alteration indices. The Ishikawa alteration index (AI) and the chlorite-carbonate-pyrite index (CCPI) are calculated in wt% [20] [21]; the carbonate saturation index (CSI) is calculated in molar proportions [22], with CO_2 derived from total carbon. Molar Na/Al and K/Al ratios locate the rocks relative to the albite (Na/Al = 1), K-feldspar (K/Al = 1) and muscovite (K/Al = 0.33) end-members [23]. The symbols in Equations (1) to (8) are defined in **Table 3**.

$$\mathrm{AI} = 100 \times \frac{\mathrm{MgO} + \mathrm{K_2O}}{\mathrm{MgO} + \mathrm{K_2O} + \mathrm{Na_2O} + \mathrm{CaO}} \tag{1}$$

$$\mathrm{CCPI} = 100 \times \frac{\mathrm{MgO} + \mathrm{FeO^T}}{\mathrm{MgO} + \mathrm{FeO^T} + \mathrm{Na_2O} + \mathrm{K_2O}} \tag{2}$$

$$\mathrm{FeO^T} = 0.8998 \times \mathrm{Fe_2O_3^T} \tag{3}$$

$$\mathrm{CSI} = \frac{\mathrm{CO_2}}{\mathrm{Ca} + \mathrm{Mg} + \mathrm{Fe}} \tag{4}$$

$$\mathrm{CO_2} = 3.664 \times \mathrm{C} \tag{5}$$

Alteration classes and reference rocks. Samples are classified according to As and S as strongly altered (As > 2000 ppm and S > 0.7%), moderately altered and least altered (As < 400 ppm and S < 0.25%); GR7, which is carbonate-rich but As-poor, is treated separately. Measuring what a rock has gained or lost requires its composition before alteration. This original rock no longer exists where alteration took place, so it is represented by a nearby least-altered sample of the same type, called here the reference rock (often termed the "precursor" in the literature). The reference rock for each altered rock belongs to the same family, identified by the Zr/TiO_2 ratio and by consistent contents of Ti, Al, Zr and Hf, which are considered poorly mobile [24].

Mass balance. Mass balances were calculated with the isocon method [25]. In the Grant diagram, each constituent is plotted using its concentration in the reference rock (x-axis) and in the altered rock (y-axis). The *isocon* is the straight line through the origin that joins the constituents whose mass did not change, *i.e.*, the immobile elements; constituents plotting above it were gained, and those plotting below it were lost. Its slope k is the mean of the C^A/C^0 ratios of the n least-mobile elements (TiO_2, Al_2O_3, Zr and Hf):

$$k = \frac{1}{n} \sum_{j=1}^{n} \frac{C_j^A}{C_j^0} \tag{6}$$

$$\frac{\Delta M}{M^0} = \frac{1}{k} - 1 \tag{7}$$

$$\frac{\Delta C_i}{C_i^0} = \frac{C_i^A - kC_i^0}{kC_i^0} \times 100 \tag{8}$$

Uncertainties. The uncertainty on the isocon slope k is estimated for each pair as the standard error of the C^A/C^0 ratios of the least-mobile elements (standard

Table 3. Symbols and parameters used in Equations (1) to (8).

Symbol	Meaning and calculation	Unit	Eq.
	Alteration indices		
AI	Ishikawa index: proportion of MgO and K_2O (sericitization, chloritization) in the sum $MgO + K_2O + Na_2O + CaO$	dimensionless (0 - 100)	(1)
CCPI	Chlorite-carbonate-pyrite index: proportion of MgO and FeO^T in the sum $MgO + FeO^T + Na_2O + K_2O$	dimensionless (0 - 100)	(2)
MgO, CaO, Na_2O, K_2O	Major oxide contents (X-ray fluorescence)	wt%	(1), (2)
FeO^T, $Fe_2O_3^T$	Total iron expressed as FeO or as Fe_2O_3 (analysed form)	wt%	(2), (3)
0.8998	$2\ M(FeO)/M(Fe_2O_3) = 2 \times 71.844/159.688$; M: molar mass	—	(3)
CSI	Carbonate saturation index: moles of CO_2 per mole of carbonate-forming cations (Ca, Mg, Fe)	dimensionless	(4)
CO_2, Ca, Mg, Fe	In (4): molar proportions = oxide content/molar mass (CO_2 44.01; CaO 56.08; MgO 40.30; FeO 71.84 g/mol)	mol/100 g	(4)
C; 3.664	Measured total carbon; $M(CO_2)/M(C) = 44.009/12.011$ (all carbon assumed to be carbonate)	wt%; —	(5)
Na/Al, K/Al	$(Na_2O/61.98)/(Al_2O_3/101.96)$ and $(K_2O/94.20)/(Al_2O_3/101.96)$; albite: Na/Al = 1; K-feldspar: K/Al = 1; muscovite: K/Al = 0.33	dimensionless	—
	Mass balance (isocon method)		
k	Isocon slope ($k = M^0/M^A$); $k < 1$: mass gain; $k > 1$: mass loss	dimensionless	(6)-(8)
n, j	Number of least-mobile elements (4: TiO_2, Al_2O_3, Zr, Hf; 3 with GR6; 2 in the TiO_2-Al_2O_3 test) and rank of each ($j = 1 \ldots n$)	—	(6)
C_j^A, C_j^0	Content of least-mobile element j in the altered rock (A) and in the reference rock (0)	wt% or ppm	(6)
M^0, M^A, ΔM	Masses of the reference rock and of the altered rock; mass change	g	(7)
i; C_i^A, C_i^0	Constituent considered; its contents in the altered rock and in the reference rock	wt% or ppm	(8)
$\Delta C_i / C_i^0$	Relative change in the amount of constituent i (>0: gain; <0: loss)	%	(8)

Variables in italics, chemical symbols in roman type. Superscript A: altered rock; superscript 0: reference rock.

deviation/$\sqrt{n}$); it ranges from 1.9% to 5.5% for the pairs studied (Section 4.4). The uncertainty on each relative change combines this term with the analytical precision of the two analyses, taken as the largest duplicate difference observed for the element group: 1.5% for the major elements (XRF), 5% for C and S, and, conservatively, 14% for the trace elements (the value reached by As, Ag and Zr). A change is interpreted only when it exceeds twice this combined uncertainty ($2u$), *i.e.*, 5% to 11% for the major elements and 28% to 30% for the trace elements with the reference rocks used (values for each pair are given in Section 4.4). With GR6, the ratios are more dispersed (standard deviation 0.21 to 0.36, mainly because of Zr); the uncertainty on k reaches 11% to 21%, and changes smaller than 23% to 42% (major elements) or 36% to 50% (trace elements) are not interpreted. The two As contents equal to the upper quantification limit (GR3, GB2) are treated as minimum values. The sensitivity of the mass balances is tested in two ways: with an isocon defined by TiO_2 and Al_2O_3 only, which removes any effect of incomplete zircon dissolution, and, for suite B, with a second reference rock (GR6).

Statistics. Associations between elements are assessed with Spearman's rank correlation coefficient (ρ, from −1 to +1), calculated on ranks, with tied values given their average rank. The five Au values of 0.001 g/t are tied, and the two As contents at the upper quantification limit (GR3, GB2), which exceed all other As values, share the two highest ranks; assigning them either order gives ρ(Au-As) = 0.66 - 0.67 and ρ(As-S) = 0.87 - 0.88. Contents below the detection limit (Te in GB3, GR5, GR6 and GR7; Tl in GR8) are ranked as tied lowest values. Because ties make tabulated critical values approximate, significance is assessed with a two-tailed permutation test (20,000 random permutations of the ranks), which keeps the tie structure of the data; the p-values are given in Section 4.5. No correction for multiple comparisons was applied, so correlations with p close to 0.05 are interpreted with caution.

4. Results

4.1. Gold Distribution in the Drill Holes

Gold is concentrated in the granitoid (Table 4), which makes up only 42% of the drilled length but 93% of the mineralized length. The metagabbros, which dominate the drilled length, are nearly barren. The metasediments contain a single interval grading more than 0.5 g/t (1.1 m at 1.14 g/t in TYD0046): it is the interval of sample GR2, logged as S3 but identified as granitoid on the core and by its chemistry (Section 3.1). The best intercept in each sampled hole is 7 to 26 m long and grades 2.1 to 6.9 g/t Au (Table 5). These proportions are based on the logged lithology (code I1C) and describe the drilled sectors, which were sited on mineralized targets; they do not replace a prospect-scale comparison between gold grades and Zr-defined lithology, which [18] recommends for establishing a lithological control.

The strongly altered samples (GR1, GR3, GR8, GB2) and GB4 lie within intercepts; GR2 occupies an isolated mineralized interval (Figure 3). The least-altered

samples, except GR6, and the carbonate-altered granitoid GR7 lie outside the intercepts, 3 to 15 m away from them (31.5 m for AR1). GR6 is a barren interval within the TYD0023 intercept, where the grade rises from less than 0.02 g/t to more than 5 g/t over 1 m.

Table 4. Gold distribution by lithology in the eleven compiled drill holes (1513 intervals).

Lithology	Intervals	Length (m)	% of length	% ≥ 0.5 g/t	Mean Au (g/t)	% of length ≥ 0.5 g/t
Granitoid (I1C)	642	647	42	34.6	0.97	92.7
Metagabbro (MI3)	706	712	47	2.3	0.05	6.8
Metasediment (S3)	153	156	10	0.7	0.01	0.5
Other (I2, S1)	12	12	1	0.0	0.002	0.0
Total	**1513**	**1527**	**100**	**15.8**	**0.44**	**100**

Log codes: I1C, granitoid; MI3, metagabbro; S3, metasediment; I2, intermediate intrusion; S1, conglomerate. Mean Au: length-weighted mean. Lithology as logged (S3B and MI3B included in S3 and MI3); the only S3 interval ≥ 0.5 g/t is that of GR2 (Section 4.1). % ≥ 0.5 g/t: proportion of the length of each lithology.

Table 5. Mineralized intercepts in the sampled drill holes and sample locations.

Drill hole	From (m)	To (m)	Length (m)	Au (g/t)	Lithology	Samples
TYD0023	44.0	52.5	8.5	4.58	I1C, MI3	GR6, GR8
TYD0023	84.0	85.0	1.0	*0.002*	*outside intercept*	*AR1 (31.5 m away)*
TYD0036	22.0	28.0	6.0	0.71	I1C, MI3	—
TYD0036	33.0	35.7	2.7	1.30	I1C, MI3	—
TYD0036	87.0	93.9	6.9	0.56	I1C, MI3	GB2
TYD0036	97.0	98.0	1.0	*0.001*	*outside intercept*	*GB1 (3.1 m away)*
TYD0036	103.3	110.3	7.0	6.94	I1C	—
TYD0046	35.0	37.7	2.7	2.66	I1C, MI3	—
TYD0046	40.4	52.5	12.1	3.30	I1C	—
TYD0046	63.6	64.7	1.1	*1.14*	*outside intercept*	*GR2 (11.1 m away)*
TYD0046	67.0	68.0	1.0	*0.001*	*outside intercept*	*GR5 (14.5 m away)*
TYD0110	88.0	90.0	2.0	4.75	MI3	GB4
TYD0110	107.0	108.0	1.0	*0.001*	*outside intercept*	*GB3 (3.0 m away)*
TYD0110	111.0	118.0	7.0	2.07	I1C, MI3	—
BBD1048	15.0	41.0	26.0	3.12	I1C	—
BBD1048	61.0	62.0	1.0	*0.001*	*outside intercept*	*GR7 (13.0 m away)*
BBD1048	75.0	86.0	11.0	2.14	I1C	GR3
BBD1000	144.0	162.0	18.0	2.71	I1C	GR1
BBD1000	168.0	169.0	1.0	*0.001*	*outside intercept*	*GR4 (4.0 m away)*
BBD1000	173.0	176.0	3.0	1.47	I1C	—
BBD1000	190.0	196.0	6.0	1.94	I1C	—

Intercepts: 0.5 g/t Au cut-off, internal dilution ≤ 2 m, length ≥ 2 m; length-weighted grades. In italics: sample intervals outside intercepts, with their grade and the distance to the nearest intercept.

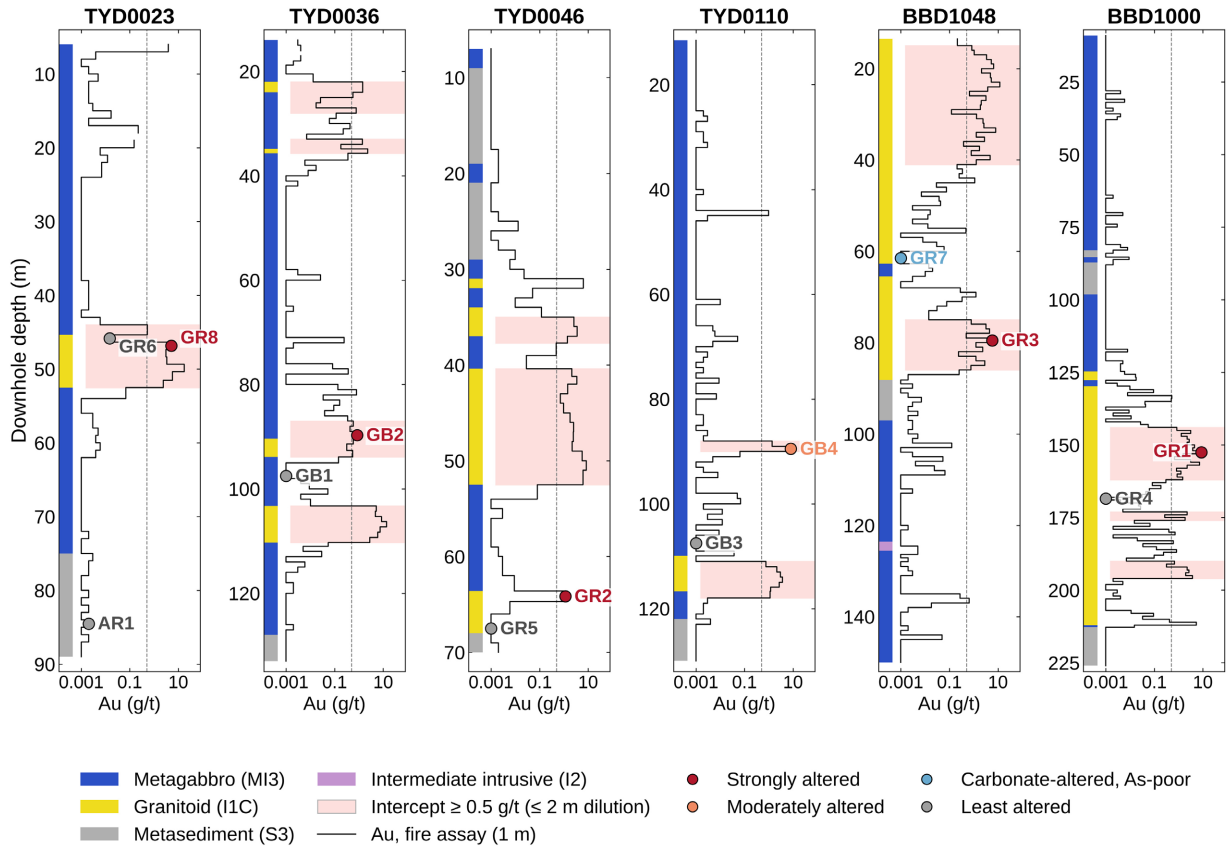

Figure 3. Gold grade profiles (1 m intervals, logarithmic scale) of the six sampled drill holes, with the lithological log (left strip), the 0.5 g/t intercepts (internal dilution ≤ 2 m; pink bands) and the sample locations. Dashed line: 0.5 g/t; downhole depths.

4.2. Geochemical Families and Reference Rocks

Ratios of least-mobile elements distinguish three families (**Table 6**; **Figure 4**): the metagabbros (Zr/TiO_2 = 30 - 44), granitoid suite A, which arenite AR1 resembles (Zr/TiO_2 = 132), and the Zr-rich suite B. GB4, like GB2, is a differentiated or silicified metagabbro [18]; its Zr/TiO_2 ratio (166) differs from that of the other metagabbros, so no reference rock of the same family could be paired with it, and no mass balance was calculated. For each pair used, the C^A/C^0 ratios of TiO_2, Al_2O_3, Zr and Hf are consistent (standard deviation ≤ 0.10), which supports the choice of reference rocks. Full compositions are given in **Table 7**.

Table 6. Geochemical families and reference rocks used for the mass balances.

Family	Zr/TiO_2	Samples	Reference rock → altered rocks
Metagabbros	30 - 44	GB1, GB2, GB3 (GB4: 166)	GB3 → GB2
Granitoids, suite A	134 - 143	GR2, GR5 (and AR1: 132)	GR5 → GR2
Granitoids, suite B (Zr-rich)	295 - 549	GR1, GR3, GR4, GR6, GR7, GR8	GR4 → GR1, GR3, GR7, GR8 (test: GR6)

For each pair, the standard deviation of the C^A/C^0 ratios of TiO_2, Al_2O_3, Zr and Hf is ≤0.10.

Table 7. Chemical composition of the samples.

	GB1	GB2	GB3	GB4	GR1	GR2	GR3	GR4	GR5	GR6	GR7	GR8	AR1
Major elements (wt%)													
SiO_2	47.99	63.32	49.49	60.45	72.79	65.60	62.37	68.88	65.00	69.27	68.49	64.77	69.77
TiO_2	1.72	1.18	1.88	0.92	0.41	0.50	0.43	0.49	0.53	0.56	0.53	0.54	0.54
Al_2O_3	12.18	5.38	11.21	11.46	8.80	12.68	9.51	10.86	13.88	11.34	10.83	11.00	13.58
$Fe_2O_3^T$	18.31	10.34	22.08	12.30	5.91	5.72	9.24	7.30	5.90	8.50	5.77	7.91	4.39
MnO	0.20	0.13	0.27	0.19	0.09	0.04	0.08	0.11	0.09	0.13	0.09	0.12	0.02
MgO	5.51	1.57	2.30	0.48	0.20	0.30	0.27	0.13	0.94	0.18	0.32	0.21	0.73
CaO	9.02	6.34	7.18	5.47	3.03	4.32	3.17	3.45	4.02	2.89	3.91	3.61	2.85
Na_2O	2.39	1.49	2.84	4.53	4.78	5.96	4.80	4.25	4.53	4.99	4.50	6.08	4.93
K_2O	0.27	0.55	0.75	0.26	0.15	0.40	0.38	1.20	1.30	0.30	0.54	0.08	1.04
P_2O_5	0.09	0.07	0.81	0.19	0.05	0.10	0.06	0.06	0.10	0.07	0.07	0.07	0.13
LOI	1.03	5.47	0.33	1.90	2.21	2.40	5.58	1.95	1.19	0.99	4.09	3.10	0.38
Total C	0.15	0.92	0.13	0.51	0.53	0.54	0.51	0.49	0.22	0.24	0.92	0.66	0.04
S	0.23	1.49	0.15	0.41	0.74	1.01	2.05	0.06	0.20	0.05	0.08	1.30	0.13
Gold (g/t)													
Au	0.001	0.837	0.001	8.12	8.64	1.14	5.82	0.001	0.001	0.015	0.001	5.15	0.002
Trace elements (ppm)													
As	330	≥10,000	125	1220	3392	2245	≥10,000	291	72	54	233	2370	85
Sb	0.51	8.74	0.19	0.40	0.79	0.96	7.37	0.12	0.23	0.14	0.14	0.66	0.14
Bi	0.75	1.05	0.07	0.14	0.32	0.25	3.29	0.38	0.10	0.04	0.05	0.27	0.17
Te	0.37	1.65	<0.05	0.06	0.13	0.14	1.26	0.07	<0.05	<0.05	<0.05	0.27	0.05
Ag	0.59	1.09	0.56	0.88	0.90	0.82	1.49	0.87	0.60	0.79	1.00	1.64	0.53
W	2.20	7.80	1.90	2.10	8.10	6.00	12.3	1.00	4.30	4.40	1.40	0.90	4.40
Mo	2.32	2.90	2.04	2.72	2.83	2.98	3.86	2.99	2.18	2.67	2.31	2.53	2.30
Pb	5.2	7.1	4.3	6.5	5.8	5.3	6.7	5.3	5.3	5.1	3.8	5.9	5.0
Cu	297	138	221	134	61.7	292	66.1	51.3	90.3	64.4	56.8	93.1	115
Zn	125	87	171	183	100	53	41	110	74	162	41	162	33
Rb	3.90	34.2	24.1	14.3	3.00	23.2	7.80	35.5	33.8	13.7	14.1	3.00	24.5
Ba	119	221	377	486	162	451	402	560	553	458	210	210	2136
Cs	0.54	7.95	7.31	2.57	0.14	3.69	0.33	3.66	2.04	3.09	1.08	0.78	1.08
Tl	0.04	0.19	0.11	0.08	0.03	0.14	0.08	0.16	0.12	0.09	0.05	<0.02	0.18
Sr	219	177	142	261	144	236	163	208	393	193	161	194	252
Zr	52.1	46.1	82.0	153	187	67.1	236	218	76.0	165	219	221	71.3
Hf	1.55	0.89	1.62	2.52	3.95	1.54	4.93	5.02	1.52	3.79	4.87	5.58	1.27

$Fe_2O_3^T$: total iron; LOI: loss on ignition. ≥10,000: upper quantification limit for As. Zr and Hf: minimum values (four-acid digestion). <: below the detection limit.

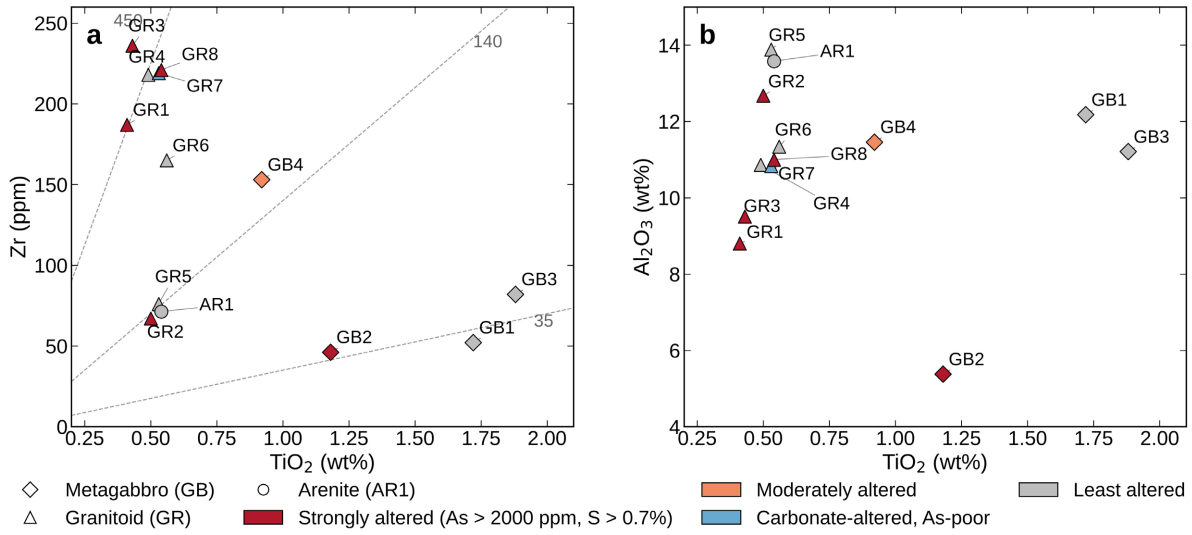

Figure 4. Identification of reference rocks using least-mobile elements: (a) Zr versus TiO_2, with lines of constant Zr/TiO_2; (b) Al_2O_3 versus TiO_2. Colours: alteration classes (Table 1).

4.3. Alteration Indices

Compared with the least-altered granitoids, the strongly altered granitoids have lower AI (2.9 - 7.5 versus 14.7 - 20.8 for GR4 and GR5), higher Na/Al (0.77 - 0.91), lower K/Al (≤0.04) and higher CSI (0.24 - 0.33) (Table 8; Figure 5). They move toward the albite end-member without trending toward muscovite, which indicates weak sericitization. Two samples are exceptions: reference rock GR4 is already weakly carbonate-altered (CSI = 0.26), and GR7 has the highest CSI (0.51) without As or S enrichment.

Table 8. Alteration indices of the samples.

Sample	AI	CCPI	Na/Al	K/Al	CSI	Na_2O/K_2O	Zr/TiO_2	Au (g/t)	Class
GB1	33.6	89.2	0.32	0.02	0.02	8.9	30	0.001	LA
GB2	21.3	84.2	0.46	0.11	0.27	2.7	39	0.837	SA
GB3	23.3	86.1	0.42	0.07	0.02	3.8	44	0.001	LA
GB4	6.9	70.7	0.65	0.02	0.16	17.4	166	8.12	MA
GR1	4.3	52.8	0.89	0.02	0.33	31.9	456	8.64	SA
GR2	6.4	46.1	0.77	0.03	0.29	14.9	134	1.14	SA
GR3	7.5	62.4	0.83	0.04	0.24	12.6	549	5.82	SA
GR4	14.7	55.1	0.64	0.12	0.26	3.5	445	0.001	LA
GR5	20.8	51.7	0.54	0.10	0.11	3.5	143	0.001	LA
GR6	5.7	59.7	0.72	0.03	0.12	16.6	295	0.015	LA
GR7	9.3	52.2	0.68	0.05	0.51	8.3	413	0.001	C
GR8	2.9	54.3	0.91	0.01	0.33	76.0	409	5.15	SA
AR1	18.5	43.9	0.60	0.08	0.02	4.7	132	0.002	LA

AI and CCPI in wt%; Na/Al, K/Al and CSI in molar proportions. Classes: see Table 1.

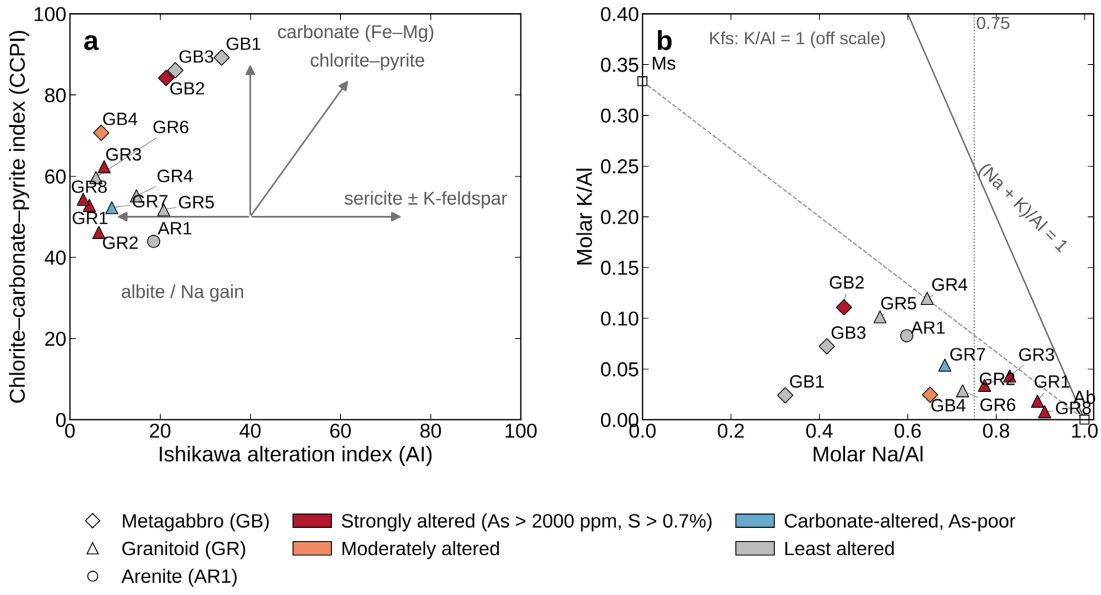

Figure 5. Alteration indices: (a) AI-CCPI diagram [21] with schematic alteration trends; (b) molar Na/Al and K/Al ratios [23], with the albite (Ab) and muscovite (Ms) end-members and the Na/Al = 0.75 threshold used for the granitoids.

4.4. Mass Balances

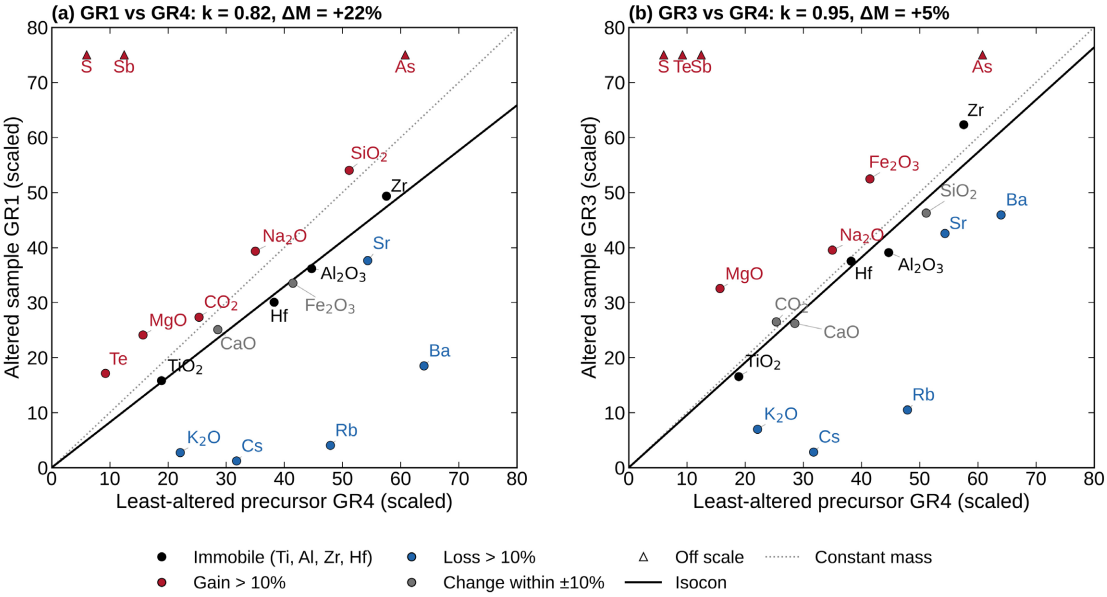

Figure 6. Isocon diagrams [25] of the mineralized granitoids GR1 (a) and GR3 (b) against reference rock GR4 (x-axis). Concentrations are multiplied by factors chosen to spread the points; triangles: off-scale values. The ±10% symbol classes are a display convention; interpretation thresholds for each pair are given in **Table 9**.

The four mineralized granitoids show the same pattern (**Table 9**; **Figure 6** and **Figure 7**): gains in Na_2O (+18% to +40%), CO_2 (except in GR3, where the +10% change is within uncertainty), S, As, Sb, Te and Ag (within uncertainty in GR1); losses in K_2O (−67% to −94%), Rb and Ba (except in GR2, where the Rb and Ba

changes are within uncertainty); the Sr decrease (−12% to −36%) exceeds the uncertainty only in GR2; and, in suite B, losses in Cs and Tl. Iron is nearly constant (−2% to +3%), except in GR3, the richest in S and As (+33%). Mass changes little (−6% to +7%), except in GR1 (+22%), which gained silica (+28%). GR7 gained CO_2 (+87%) and lost K_2O (−56%), Rb and Ba, with no As gain (−21%) and a modest S gain (+45%) from a very low starting S content (0.06% to 0.08%). Metagabbro GB2 shows the largest changes: a mass gain of about 80%, mostly due to silica (+131%) and carbonate, with additions of S, As, Sb, Te and W and, unlike the granitoids, a gain in K_2O (+32%).

Table 9. Mass balances: relative changes (%) in the altered rocks relative to their reference rock (isocon method).

Constituent	GR1	GR3	GR8	GR2	GR7	GB2
Reference rock	*GR4*	*GR4*	*GR4*	*GR5*	*GR4*	*GB3*
Isocon slope *k*	0.82	0.95	1.06	0.94	1.01	0.55
Mass change ΔM (%)	+22	+5	−6	+7	−1	+80
Uncertainty on k (%)	1.9	5.2	2.6	3.0	2.4	5.5
Threshold 2u, major/trace elements (%)	5/28	11/30	6/28	7/29	6/28	11/30
SiO_2	+28	−5	−11	+8	−2	+131
Al_2O_3	−2	−8	−4	−3	−2	−13
$Fe_2O_3^T$	−2	+33	+2	+3	−22	−16
MgO[a]	+87	+118	+52	−66	+143	+23
CaO	+7	−4	−1	+15	+12	+59
Na_2O	+37	+18	+35	+40	+4	−5
K_2O	−85	−67	−94	−67	−56	+32
CO_2	+31	+10	+28	+158	+87	+1152
S	+1537	+3805	+2130	+433	+45	+1667
As[a]	+1316	≥+3500	+668	+3223	−21	≥+14320
Sb[a]	+700	+6335	+419	+345	+15	+8191
Te[a]	+126	+1786	+264	≥+198	≤−30	≥+5848
Ag	+26	+79	+78	+46	+13	+251
W	+884	+1189	−15	+49	+38	+640
Rb	−90	−77	−92	−27	−61	+156
Ba	−65	−25	−65	−13	−63	+6
Sr	−16	−18	−12	−36	−24	+125
Cs	−95	−91	−80	+93	−71	+96
Tl	−77	−48	≤−88	+24	−69	+211
Pb	+33	+32	+5	+7	−29	+198
Cu	+46	+35	+71	+245	+9	+13
Zn	+10	−61	+39	−24	−63	−8

Changes smaller than the threshold 2u (twice the combined uncertainty of k and of the analyses; Section 3.3) are not interpreted; for CO_2 and S, 2u = 11% - 15%. [a]Constituents present at very low levels in the reference rock: high relative uncertainty. As in GR3 and GB2: minimum values (quantification limit). Tl in GR8: below the detection limit. Te below the detection limit in GR5, GR7 and GB3: minimum (≥) or maximum (≤) values.

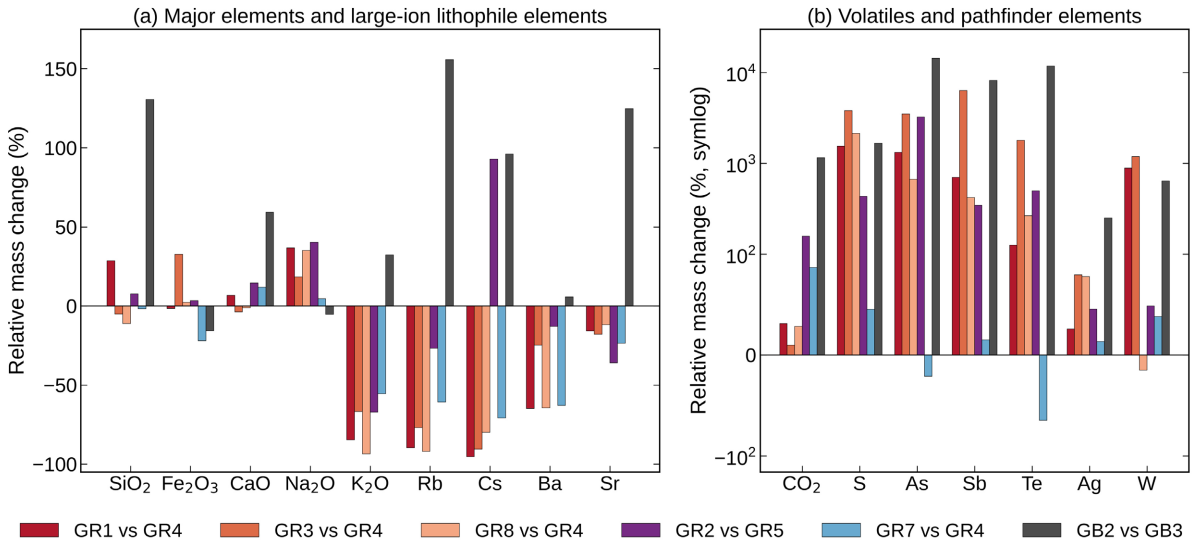

Figure 7. Relative mass changes (%) with respect to the reference rocks: (a) major and lithophile elements; (b) CO_2, S and pathfinder elements (symmetric log scale, linear between −100% and +100% and logarithmic beyond). Interpretation thresholds for each pair are given in Table 9.

Defining the isocon with TiO_2 and Al_2O_3 only, which removes the effect of incomplete zircon dissolution, does not change the interpretation. With GR4 and GR5 as reference rocks, k changes by less than 3%, except for GR3 (0.88 instead of 0.95); the Na_2O gains (+29% to +42%), the K_2O losses (−64% to −94%) and the gains in CO_2, S and As keep the same direction and similar magnitudes, and the mass balances of GR7 and GB2 change by no more than 5 percentage points.

With GR6 as the reference rock and the isocon defined by TiO_2, Al_2O_3 and Zr, the ratios are dispersed (standard deviation 0.21 to 0.36), because the Zr ratio (1.13 to 1.43) departs from those of TiO_2 and Al_2O_3 (0.73 to 0.97); the uncertainty on k is then 11% to 21% (Section 3.3). The gains in S, As and CO_2 and the Cs losses remain beyond uncertainty, and Rb and Ba decrease in all three rocks, although the smallest of these losses fall within the larger uncertainty (Table 10); but the Na_2O change (−5% to +12%) is within uncertainty and the K_2O change is variable (−76% to +25%). With TiO_2 and Al_2O_3 only, the GR6 ratios agree closely (differences ≤ 0.07): the Na_2O gain reappears (+20% to +27%), whereas the K_2O change remains variable (−72% to +58%), because GR6, which lies within the TYD0023 intercept, is itself K-poor (K/Al = 0.03). The low Zr of GR6 relative to TiO_2 (Zr/TiO_2 = 295, the lowest value of suite B) may reflect a different original composition or a lower zircon recovery; in either case, the GR6 results depend on Zr. The direction of the transfers is therefore robust, the Na_2O gain is confirmed when Zr is excluded, and only the magnitude of the K_2O loss depends on the reference rock.

4.5. Pathfinder Elements and Gold Grades

As, S, Sb, Te, Bi, Pb and Ag vary together (ρ with As from 0.74 to 0.88; Table 11;

Figure 8), whereas Cu and Zn are not associated with them. Gold follows As, S, Sb, Pb, Ag and Na/Al, and varies inversely with K_2O and AI. The six As-anomalous samples grade 0.84 to 8.64 g/t Au, whereas the other seven, including the three reference rocks and GR7, grade no more than 0.015 g/t. A high CSI alone does not indicate mineralization (GR4, GR7). Table 12 summarizes the results of Sections 4.4 and 4.5.

Table 10. Sensitivity of the mass balances to the choice of reference rock and of least-mobile elements (GR1, GR3 and GR8; changes in %).

Constituent	Relative to GR4	Relative to GR6 (TiO_2, Al_2O_3, Zr)	Relative to GR6 (TiO_2, Al_2O_3)
Na_2O	+18 to +37	−5 to +12	+20 to +27
K_2O	−94 to −67	−76 to +25	−72 to +58
CO_2	+10 to +31	+108 to +151	+162 to +188
S	+1537 to +3805	+1691 to +4209	+1991 to +5330
Rb	−92 to −77	−80 to −44	−77 to −29
Cs	−95 to −80	−95 to −77	−94 to −74
Ba	−65 to −25	−60 to −13	−53 to +9
Standard deviation of isocon ratios	≤0.10	0.21 - 0.36	≤0.05

Isocon defined by TiO_2, Al_2O_3, Zr and Hf (GR4), by TiO_2, Al_2O_3 and Zr (GR6), or by TiO_2 and Al_2O_3 only (last column). As and S increase strongly in all cases.

Table 11. Spearman correlation coefficients (ρ) with gold and arsenic, and their significance (p) (n = 13).

Variable	ρ with Au (p)	ρ with As (p)
As	**0.67** (0.017)	—
S	**0.65** (0.020)	**0.88** (<0.001)
Sb	**0.63** (0.030)	**0.84** (<0.001)
Te	0.46 (0.12)	**0.87** (<0.001)
Bi	0.31 (0.30)	**0.79** (0.002)
Ag	**0.56** (0.048)	**0.74** (0.006)
Pb	**0.70** (0.011)	**0.79** (0.002)
Mo	0.55 (0.056)	**0.68** (0.011)
W	0.49 (0.096)	0.37 (0.21)
Cu	−0.01 (0.98)	0.13 (0.66)
Zn	0.09 (0.78)	−0.08 (0.81)
CO_2	0.44 (0.14)	**0.67** (0.023)
Molar Na/Al	**0.70** (0.012)	0.38 (0.20)
K_2O	**−0.69** (0.012)	−0.48 (0.099)
AI index	**−0.71** (0.009)	−0.24 (0.42)

Bold: $p < 0.05$. p: two-tailed permutation test (20,000 permutations of the ranks, ties given their average rank, n = 13).

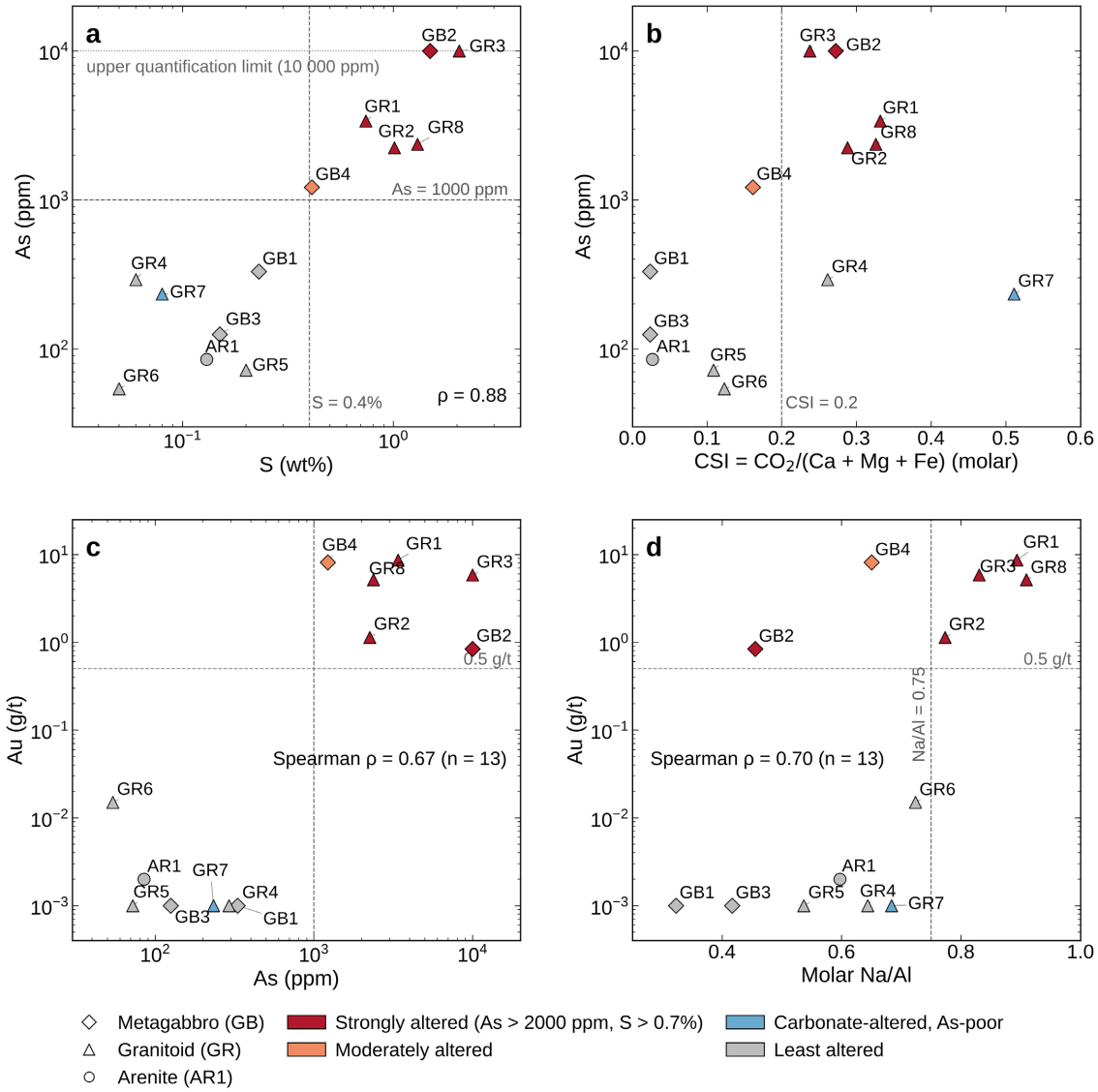

Figure 8. Pathfinder elements and gold grades: (a) As-S; (b) As-CSI; (c) Au-As; (d) Au-Na/Al. Dashed lines: thresholds in Table 13 and 0.5 g/t Au; dotted lines: upper quantification limit for As.

Table 12. Summary of mass balances and of relationships between pathfinder elements and gold.

Parameter	Mineralized granitoids (GR1, GR2, GR3, GR8)	GR7 (carbonate-altered, As-poor)	Metagabbro GB2
	Mass balances **(Table 9 and Table 10)**		
Mass change	−6% to +22% (silica in GR1: SiO_2 +28%)	−1%	+80% (SiO_2 +131%)
Gains	Na_2O +18% to +40%; CO_2 +28% to +158% (GR3: +10%, within uncertainty); S, As, Sb, Te, Ag	CO_2 +87%; no As gain	CO_2, S, As, Sb, Te, W
Losses	K_2O −67% to −94%; Rb, Ba; Cs and Tl (suite B); Sr only in GR2	K_2O −56%; Rb; Ba	Minor (Al_2O_3, $Fe_2O_3^T$)
Iron ($Fe_2O_3^T$)	Nearly constant (−2% to +3%), except GR3 (+33%)	−22%	−16%
Reference rock GR6	S, As, CO_2, Rb, Cs, Ba: same direction; Na_2O −5% to +12% (TiO_2-Al_2O_3-Zr isocon) but +20% to +27% (TiO_2-Al_2O_3 isocon); K_2O −76% to +58%: only the magnitude of the K loss depends on the reference rock		

Continued

Pathfinder elements and gold (Table 11)	
Association	As, S, Sb, Te, Bi, Pb and Ag vary together (ρ with As: 0.74 - 0.88); Cu and Zn not associated
Correlations with Au	Positive: Pb, Na/Al (0.70), As (0.67), S (0.65), Sb (0.63), Ag (0.56); negative: AI (−0.71), K_2O (−0.69)
Gold grades	6 As-anomalous samples: 0.84 - 8.64 g/t; 7 others: ≤0.015 g/t; high CSI alone does not indicate gold (GR4, GR7)

Reference rocks: GR4 (suite B), GR5 (GR2), GB3 (GB2).

5. Discussion

5.1. Nature of the Gold-Related Alteration

The mass balances define three transfers. The first, seen in the granitoids, is sodic: gain in Na, loss in K, Rb and Ba, and a position close to the albite end-member. It is consistent with the replacement of K-feldspar and biotite by albite, as summarized by Reaction (9). This albitization is inferred from the chemistry and still needs to be confirmed in thin section, and its extent is uncertain because the suite B granitoids are already sodic. The Na gain is in line with the caveat raised in [18]: alkali alteration may have enhanced the trondhjemitic character of the normative classification, which should therefore rely preferably on the least-mobile elements. It is also consistent with the albite-bearing assemblage described at Bomboré [11] [12] and contrasts with the sericitization common in orogenic gold deposits [6]. In Burkina Faso, Na_2O enrichment also accompanies the gold-bearing granodiorite at Napélépéra [26], whereas at Kiaka gold is associated with potassic alteration and Na loss [27]; sodic alteration has also been described at Tabakoto, Mali [28]. The second transfer is carbonatization (CO_2 addition, high CSI) and the third is sulfidation (S, As, Sb, Te, Ag). Silicification is local (GR1, GB2) and agrees with the silica enrichment of the mineralized metagabbros described in [18].

$$KAlSi_3O_8 + Na^+ \rightarrow NaAlSi_3O_8 + K^+ \quad (9)$$

In Reaction (9), $KAlSi_3O_8$ is K-feldspar, $NaAlSi_3O_8$ is albite, and Na^+ and K^+ are ions dissolved in the fluid: sodium is supplied by the fluid and the released potassium passes into it, which matches the measured pairing of Na gain and K loss.

The combined addition of CO_2, S and Na, the As-Sb-Te-Bi-Ag association and the lack of correlation between gold and Cu or Zn are consistent with a reduced, sulfur-bearing aqueous-carbonic fluid, as in most orogenic gold systems [2]-[4]. A comparable signature was obtained from mass balances at the Esaase deposit in Ghana [29]. Our data cannot establish the source of the sodium or the number of fluid events; sulfide chemistry, as applied in the Mana district [30], could resolve these points.

5.2. Gold Deposition

In the mineralized granitoids, sulfur increases sharply while iron remains nearly constant, except in GR3. This combination suggests that sulfur was fixed as sulfides by iron already present in the rock, at the expense of the Fe-bearing minerals

(Reaction (10)). This sulfidation consumes H_2S from the fluid and destabilizes the gold bisulfide complexes, causing gold to precipitate (Reaction (11)) [3] [7].

$$FeO_{(rock)} + 2H_2S_{(aq)} \rightarrow FeS_2 + H_2O + H_{2(aq)} \quad (10)$$

$$Au(HS)_2^- + H^+ + 1/2\,H_{2(aq)} \rightarrow Au + 2H_2S_{(aq)} \quad (11)$$

In these reactions, $FeO_{(rock)}$ represents the ferrous iron of the silicates and oxides of the host rock, FeS_2 is pyrite, $Au(HS)_2^-$ is the gold bisulfide complex, and the subscript (aq) denotes a species dissolved in the fluid. Reaction (10) lowers the activity of H_2S, which shifts the equilibrium of Reaction (11) to the right. The suite B granitoids are Fe-rich for felsic rocks (5.8% to 9.2% $Fe_2O_3^T$) and are therefore well suited to this mechanism, which remains to be tested by studying the sulfides and the textural position of gold.

5.3. Alteration Zoning

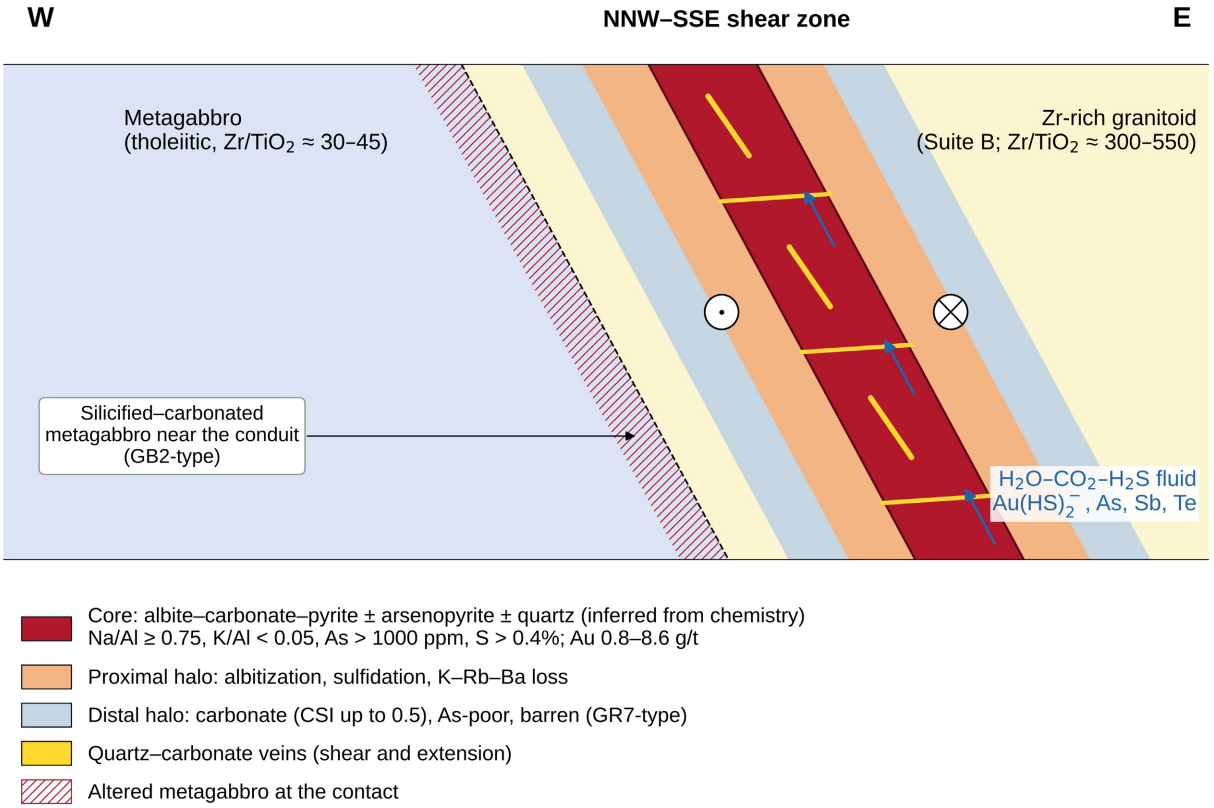

Figure 9. Schematic model of alteration zoning around a NNW-SSE shear zone (section looking north, not to scale). Mineral assemblages are inferred from the chemistry and must be confirmed by petrography; the sinistral sense of the strike-slip component is inferred from the mean planes and remains provisional [18].

The drill-hole profiles allow a tentative zoning to be outlined (**Figure 9**). The sulfide signature hardly extends beyond the mineralized intervals: in TYD0036,

TYD0110 and BBD1000, the least-altered rocks 3 or 4 m from the intercepts are poor in As and S. Carbonatization extends farther (GR7, 13 m from an intercept), and GR6, which is barren but lies within the TYD0023 intercept, is already K-poor (K/Al = 0.03), which may reflect K loss. The change from a barren interval to one grading more than 5 g/t over 1 m suggests that gold deposition is controlled at the metre scale, probably by vein and fracture density [31].

5.4. Exploration Vectors

Table 13 lists criteria that can be applied to routine analyses. In this dataset, the combination As > 1000 ppm and S > 0.4% separates the six mineralized samples from the seven barren ones, and in the granitoids Na/Al ≥ 0.75 gives the same separation. K/Al and CSI may indicate haloes wider than the mineralized core, but on their own they do not separate the samples (Figure 10). Because the thresholds were selected and evaluated on the same, deliberately sampled material, these results do not establish their predictive reliability elsewhere; they need to be tested by systematic sampling across the mineralized zones.

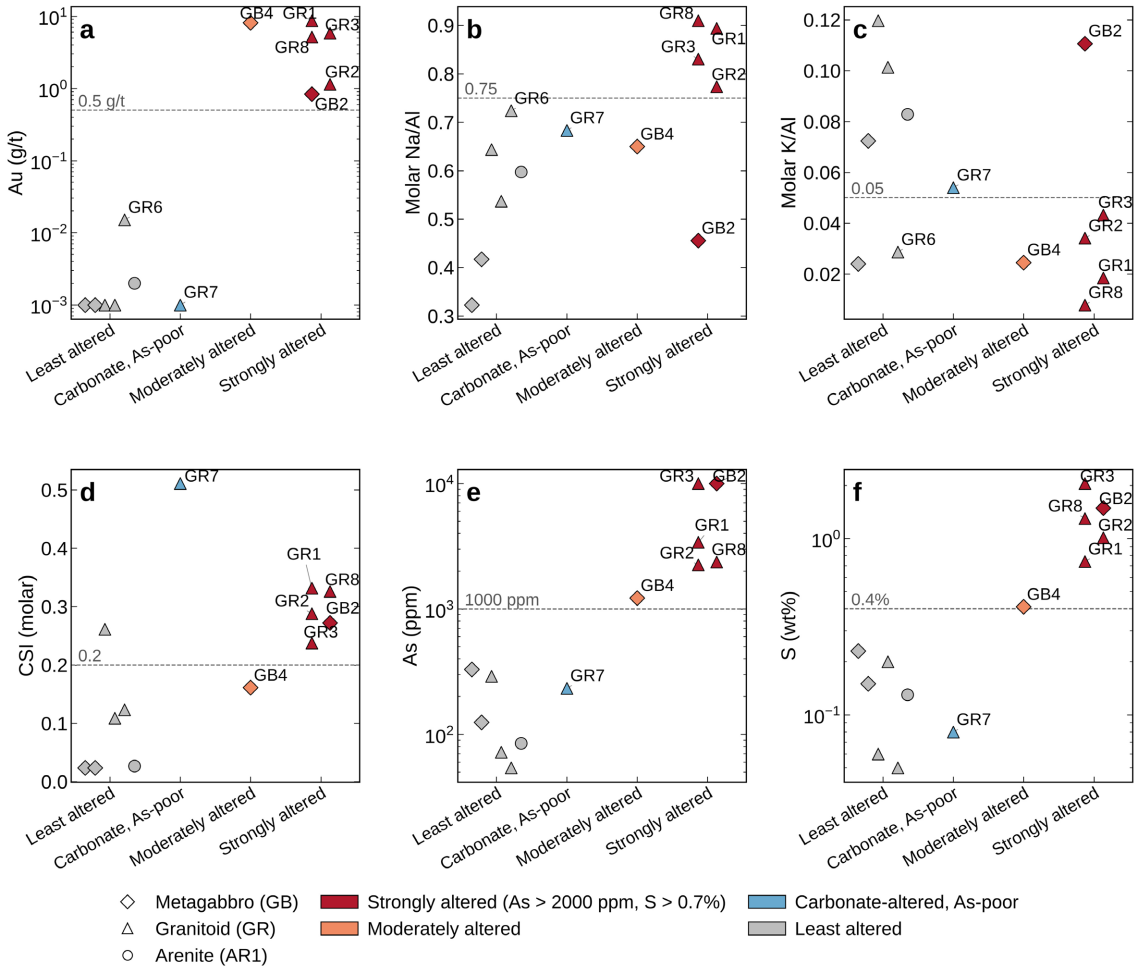

Figure 10. Distribution of the geochemical vectors by alteration class: (a) Au; (b) Na/Al; (c) K/Al; (d) CSI; (e) As; (f) S. Dashed lines: thresholds in Table 13.

Table 13. Proposed geochemical exploration vectors (indicative thresholds, n = 13).

Criterion	Threshold	Meaning	Use
As and S	>1000 ppm and >0.4%	Mineralized sulfide core: separates the 6 mineralized from the 7 barren samples of this dataset	All rock types
Molar Na/Al	≥0.75	Proximal albitization	Granitoids
Molar K/Al	<0.05	K loss; halo wider than the core	With As and S
CSI	>0.2	Carbonatization; wider halo, not correlated with gold	With As and S
Zr/TiO_2	>290	Zr-rich host unit (ratio little affected by alteration)	Granitoids

GB4 (S = 0.41%) lies just above the S threshold, which needs to be confirmed by denser sampling.

6. Conclusion

At the Toéyoko prospect, gold is associated with sodic, carbonate and sulfide alteration, developed mainly in the granitoids that host most of the mineralized zone. The mineralized granitoids lost K, Rb and Ba, and also Cs in suite B, and gained CO_2, S, As, Sb, Te and Ag. Their Na gain is recovered with both reference rocks when the isocon is defined by Ti and Al, whereas the magnitude of the K loss depends on the reference rock. These element transfers are consistent with a reduced, sulfur-bearing aqueous-carbonic fluid, and gold most likely precipitated during sulfidation of host-rock iron. The sulfur-rich zone is narrow, whereas K loss and carbonatization extend farther out. For exploration, As and S, combined with Na/Al in the granitoids, outline the mineralized core in the samples studied. Petrography, sulfide chemistry and regular sampling across the shear zones are needed to test this model.

Author Contributions

Madi OUEDRAOGO: conceptualization, sampling, core logging, data curation, formal analysis, writing (original draft). Gounwendmanaghré Hubert ZONGO: supervision, interpretation of the geology of the Bomboré district, writing (review and editing). Pascal OUIYA: methodology, interpretation of the geochemical data, writing (review and editing). Ernest Gomdebziige OUEDRAOGO: validation, writing (review and editing). Saga SAWADOGO: interpretation, validation, writing (review and editing). Seta NABA: supervision, project administration, writing (review and editing). All authors have read and approved the final version of the manuscript.

Acknowledgements

The authors thank Orezone Gold Corporation for access to the drill-hole data, core and maps, and Université Joseph Ki-Zerbo, Université Yembila Abdoulaye TOGUYENI and École Normale Supérieure for their support.

Conflicts of Interest

The authors declare no conflicts of interest regarding the publication of this paper.

References

[1] Groves, D.I., Goldfarb, R.J., Gebre-Mariam, M., Hagemann, S.G. and Robert, F. (1998) Orogenic Gold Deposits: A Proposed Classification in the Context of Their Crustal Distribution and Relationship to Other Gold Deposit Types. *Ore Geology Reviews*, **13**, 7-27. https://doi.org/10.1016/s0169-1368(97)00012-7

[2] McCuaig, T. and Kerrich, R. (1998) P-T-t-Deformation-Fluid Characteristics of Lode Gold Deposits: Evidence from Alteration Systematics. *Ore Geology Reviews*, **12**, 381-453. https://doi.org/10.1016/s0169-1368(98)00010-9

[3] Phillips, G.N. and Powell, R. (2010) Formation of Gold Deposits: A Metamorphic Devolatilization Model. *Journal of Metamorphic Geology*, **28**, 689-718. https://doi.org/10.1111/j.1525-1314.2010.00887.x

[4] Goldfarb, R.J. and Pitcairn, I. (2022) Orogenic Gold: Is a Genetic Association with Magmatism Realistic? *Mineralium Deposita*, **58**, 5-35. https://doi.org/10.1007/s00126-022-01146-8

[5] Meyer, F.M. (2023) Case Histories of Orogenic Gold Deposits. *Minerals*, **13**, Article 369. https://doi.org/10.3390/min13030369

[6] Eilu, P. and Groves, D.I. (2001) Primary Alteration and Geochemical Dispersion Haloes of Archaean Orogenic Gold Deposits in the Yilgarn Craton: The Pre-Weathering Scenario. *Geochemistry*: *Exploration*, *Environment*, *Analysis*, **1**, 183-200. https://doi.org/10.1144/geochem.1.3.183

[7] Mikucki, E.J. (1998) Hydrothermal Transport and Depositional Processes in Archean Lode-Gold Systems: A Review. *Ore Geology Reviews*, **13**, 307-321. https://doi.org/10.1016/s0169-1368(97)00025-5

[8] Goldfarb, R.J., André-Mayer, A., Jowitt, S.M. and Mudd, G.M. (2017) West Africa: The World's Premier Paleoproterozoic Gold Province. *Economic Geology*, **112**, 123-143. https://doi.org/10.2113/econgeo.112.1.123

[9] Masurel, Q., Eglinger, A., Thébaud, N., Allibone, A., André-Mayer, A., McFarlane, H., *et al.* (2022) Paleoproterozoic Gold Events in the Southern West African Craton: Review and Synopsis. *Mineralium Deposita*, **57**, 513-537. https://doi.org/10.1007/s00126-021-01052-5

[10] Perret, J., Jessell, M.W., Masurel, Q., Hayman, P.C., Thébaud, N., Baratoux, L., *et al.* (2025) Review of Paleoproterozoic Tectonics in the Southern West African Craton: Insights from Multi-Disciplinary Data Integration. *Precambrian Research*, **422**, Article ID: 107707. https://doi.org/10.1016/j.precamres.2025.107707

[11] Zongo, G.H. (2017) Caractérisation du gisement aurifère de Bomboré: Pétrographie, géochimie, déformation, altération hydrothermale et minéralisation (Burkina Faso, Afrique de l'Ouest). Ph.D. Thesis, Université Ouaga I Pr Joseph Ki-Zerbo.

[12] Orezone Gold Corporation (2023) Bomboré Phase II Expansion, Burkina Faso, West Africa: Definitive Feasibility Study. NI 43-101 Technical Report, Effective Date 28 March 2023.

[13] Parra-Avila, L.A., Kemp, A.I.S., Fiorentini, M.L., Belousova, E., Baratoux, L., Block, S., *et al.* (2017) The Geochronological Evolution of the Paleoproterozoic Baoulé-Mossi Domain of the Southern West African Craton. *Precambrian Research*, **300**, 1-27. https://doi.org/10.1016/j.precamres.2017.07.036

[14] Béziat, D., Dubois, M., Debat, P., Nikiéma, S., Salvi, S. and Tollon, F. (2008) Gold Metallogeny in the Birimian Craton of Burkina Faso (West Africa). *Journal of African Earth Sciences*, **50**, 215-233. https://doi.org/10.1016/j.jafrearsci.2007.09.017

[15] Baratoux, L., Metelka, V., Naba, S., Jessell, M.W., Grégoire, M. and Ganne, J. (2011) Juvenile Paleoproterozoic Crust Evolution during the Eburnean Orogeny (~2.2-2.0 Ga), Western Burkina Faso. *Precambrian Research*, **191**, 18-45. https://doi.org/10.1016/j.precamres.2011.08.010

[16] Chardon, D., Bamba, O. and Traoré, K. (2020) Eburnean Deformation Pattern of Burkina Faso and the Tectonic Significance of Shear Zones in the West African Craton. *BSGF—Earth Sciences Bulletin*, **191**, Article No. 2. https://doi.org/10.1051/bsgf/2020001

[17] Chardon, D., Traoré, K., Gumiaux, C. and Naba, S. (2026) Transpressional Flow and Escape of Orogens: The Paleoproterozoic Eburnean Accretionary Orogen of West Africa. *Journal of Structural Geology*, **210**, Article ID: 105742. https://doi.org/10.1016/j.jsg.2026.105742

[18] Ouedraogo, M., Zongo, G.H., Ouiya, P., Ouedraogo, E.G., Sawadogo, S. and Naba, S. (2026) Factors Controlling Gold Mineralization at the Toéyoko Prospect (P17-P17 South), Bomboré District, Burkina Faso: A Structural and Host-Rock Lithogeochemical Approach. *Open Journal of Geology*, **16**, 765-790. https://doi.org/10.4236/ojg.2026.1611037

[19] Castaing, C., Billa, M., Milési, J.P., Thiéblemont, D., Le Métour, J., Egal, E., Donzeau, M., *et al.* (2003) Notice explicative de la carte géologique et minière du Burkina Faso à l'échelle 1/1 000 000. BRGM.

[20] Ishikawa, Y., Sawaguchi, T., Iwaya, S. and Horiuchi, M. (1976) Delineation of Prospecting Targets for Kuroko Deposits Based on Modes of Volcanism of Underlying Dacite and Alteration Halos. *Mining Geology*, **26**, 105-117.

[21] Large, R.R., Gemmell, J.B., Paulick, H. and Huston, D.L. (2001) The Alteration Box Plot: A Simple Approach to Understanding the Relationship between Alteration Mineralogy and Lithogeochemistry Associated with Volcanic-Hosted Massive Sulfide Deposits. *Economic Geology*, **96**, 957-971. https://doi.org/10.2113/96.5.957

[22] Kishida, A. and Kerrich, R. (1987) Hydrothermal Alteration Zoning and Gold Concentration at the Kerr-Addison Archean Lode Gold Deposit, Kirkland Lake, Ontario. *Economic Geology*, **82**, 649-690. https://doi.org/10.2113/gsecongeo.82.3.649

[23] Davies, J.F. and Whitehead, R.E. (2006) Alkali-Alumina and MgO-Alumina Molar Ratios of Altered and Unaltered Rhyolites. *Exploration and Mining Geology*, **15**, 75-88. https://doi.org/10.2113/gsemg.15.1-2.75

[24] MacLean, W.H. and Kranidiotis, P. (1987) Immobile Elements as Monitors of Mass Transfer in Hydrothermal Alteration; Phelps Dodge Massive Sulfide Deposit, Matagami, Quebec. *Economic Geology*, **82**, 951-962. https://doi.org/10.2113/gsecongeo.82.4.951

[25] Grant, J.A. (1986) The Isocon Diagram; a Simple Solution to Gresens' Equation for Metasomatic Alteration. *Economic Geology*, **81**, 1976-1982. https://doi.org/10.2113/gsecongeo.81.8.1976

[26] Ouédraogo, T., Sawadogo, S., Ilboudo, H. and Naba, S. (2023) Alteration Typology and Geochemical Signatures of the Napélépéra Gold-Bearing Granodiorite in South-West Burkina Faso (West Africa). *Open Journal of Geology*, **13**, 1162-1175. https://doi.org/10.4236/ojg.2023.1310049

[27] Sawadogo, B., Zongo, G.H., Bonzi, W.M., Traore, K., Sawadogo, S., Yameogo, O., *et*

al. (2024) Hydrothermal Alteration Associated with the Kiaka World-Class Gold Deposit (Burkina Faso, West Africa). *Open Journal of Geology*, **14**, 989-1015. https://doi.org/10.4236/ojg.2024.1412044

[28] Diallo, M., Salvi, S., Baratoux, L., Béziat, D., Vanderhaeghe, O., Labou, I., *et al.* (2024) Geology of the Tabakoto Gold Deposit, Kédougou-Kéniéba Inlier, West African Craton, Mali. *BSGF—Earth Sciences Bulletin*, **195**, Article 24. https://doi.org/10.1051/bsgf/2024024

[29] Agyenim, B. and Adomako-Ansah, K. (2026) Alteration and Lithogeochemical Characterisation of the Esaase Gold Deposit in the Paleoproterozoic Birimian Terrane of Ghana. *Applied Earth Science: Transactions of the Institutions of Mining and Metallurgy*, **135**, 101-117. https://doi.org/10.1177/25726838251405980

[30] Augustin, J. and Gaboury, D. (2019) Multi-Stage and Multi-Sourced Fluid and Gold in the Formation of Orogenic Gold Deposits in the World-Class Mana District of Burkina Faso—Revealed by LA-ICP-MS Analysis of Pyrites and Arsenopyrites. *Ore Geology Reviews*, **104**, 495-521. https://doi.org/10.1016/j.oregeorev.2018.11.011

[31] Tavares Nassif, M., Monecke, T., Reynolds, T.J., Kuiper, Y.D., Goldfarb, R.J., Piazolo, S., *et al.* (2022) Formation of Orogenic Gold Deposits by Progressive Movement of a Fault-Fracture Mesh through the Upper Crustal Brittle-Ductile Transition Zone. *Scientific Reports*, **12**, Article No. 17379. https://doi.org/10.1038/s41598-022-22393-9